ADVANCED BIOLOGY
www.advanced-bio.com

High-Yield Production, Characterization, and Functionalization of Recombinant Magnetosomes in the Synthetic Bacterium *Rhodospirillum rubrum "magneticum"*

*Frank Mickoleit, Sabine Rosenfeldt, Mauricio Toro-Nahuelpan, Miroslava Schaffer, Anna S. Schenk, Jürgen M. Plitzko, and Dirk Schüler**

Recently, the photosynthetic *Rhodospirillum rubrum* has been endowed with the ability of magnetosome biosynthesis by transfer and expression of biosynthetic gene clusters from the magnetotactic bacterium *Magnetospirillum gryphiswaldense*. However, the growth conditions for efficient magnetite biomineralization in the synthetic *R. rubrum "magneticum"*, as well as the particles themselves (i.e., structure and composition), have so far not been fully characterized. In this study, different cultivation strategies, particularly the influence of temperature and light intensity, are systematically investigated to achieve optimal magnetosome biosynthesis. Reduced temperatures ≤16 °C and gradual increase in light intensities favor magnetite biomineralization at high rates, suggesting that magnetosome formation might utilize cellular processes, cofactors, and/or pathways that are linked to photosynthetic growth. Magnetosome yields of up to 13.6 mg magnetite per liter cell culture are obtained upon photoheterotrophic large-scale cultivation. Furthermore, it is shown that even more complex, i.e., oligomeric, catalytically active functional moieties like enzyme proteins can be efficiently expressed on the magnetosome surface, thereby enabling the in vivo functionalization by genetic engineering. In summary, it is demonstrated that the synthetic *R. rubrum "magneticum"* is a suitable host for high-yield magnetosome biosynthesis and the sustainable production of genetically engineered, bioconjugated magnetosomes.

1. Introduction

Magnetosomes are biogenic magnetic nanoparticles biomineralized by magnetotactic bacteria (MTB). For example, the well-studied alphaproteobacterium *Magnetospirillum gryphiswaldense* typically produces 15–25 cuboctahedral particles of chemically pure magnetite (Fe_3O_4). Within the cells, the particles are arranged in linear chains, thereby forming an intracellular "compass needle" for navigation along geomagnetic field lines. Magnetosome biosynthesis is compartmentalized within vesicles of the magnetosome membrane that provide confined "nanoreactors" in which the physico-chemical conditions are strictly regulated by a set of specific proteins.[1,2] These exert precise control over different stages of biomineralization,[3] which results in well-defined magnetic nanoparticles with uniform shapes and sizes, high crystallinity, and strong magnetization.[4–6]

As magnetite is a mixed-valence iron oxide, concise redox control is crucial for magnetosome biosynthesis. In *M. gryphiswaldense,* magnetite biomineralization is

F. Mickoleit, M. Toro-Nahuelpan,[+] D. Schüler
Dept. Microbiology
University of Bayreuth
D-95447 Bayreuth, Germany
E-mail: dirk.schueler@uni-bayreuth.de

The ORCID identification number(s) for the author(s) of this article can be found under https://doi.org/10.1002/adbi.202101017.

[+]Present address: EMBL Heidelberg, Structural and Computational Biology Unit, D-69117 Heidelberg, Germany

DOI: 10.1002/adbi.202101017

S. Rosenfeldt
Bavarian Polymer Institute (BPI)/Physical Chemistry 1
University of Bayreuth
D-95447 Bayreuth, Germany

M. Toro-Nahuelpan, M. Schaffer, J. M. Plitzko
Dept. Molecular Structural Biology
Max Planck Institute of Biochemistry
D-82152 Martinsried, Germany

A. S. Schenk
Bavarian Polymer Institute (BPI)/Physical Chemistry – Colloidal Systems
University of Bayreuth
D-95447 Bayreuth, Germany

induced under micro- to anoxic conditions. Thereby, decreasing oxygen levels were found to stimulate particle formation, and in the entire absence of oxygen with nitrate (NO_3^-) as the only electron acceptor for respiration the highest quantities and largest magnetite crystals were produced. It can be assumed that these micro-/anoxic conditions directly affect the physico-chemical conditions within the magnetosome vesicles, and favor magnetite biomineralization.[7–11] Magnetosomes can be isolated and purified from disrupted cells by magnetic separation, which is often followed by density-based ultracentrifugation.[12–14]

Because of their unprecedented characteristics, isolated magnetosomes have been envisioned for several biotechnological and biomedical applications. For instance, magnetosomes were successfully tested as contrast agents for the two preeminent magnetic imaging techniques magnetic resonance imaging and magnetic particle imaging.[6,15–18] Further envisioned implementations include their usage for magnetic hyperthermia,[19–21] as drug carriers,[22,23] or as detection devices for protein components.[24,25] Moreover, the range of potential applications was shown to be further enhanced/expanded by the coupling to functional moieties. In the magnetic bacteria *M. gryphiswaldense* and *M. magneticum*, foreign "cargo" proteins and peptides such as fluorophores, enzymes, nanobodies (camelid antibody fragments), or versatile coupling groups were expressed on the particle surface as genetic fusions to abundant magnetosome membrane (Mam) proteins.[26–29] In addition, magnetic nanoparticles with several genetically encoded functionalities were produced by the use of tandem fusions and multiple magnetosome membrane anchors.[30,31]

However, despite of recent progress in the development of optimized fermentation methods for *M. gryphiswaldense*,[11,32–34] large scale cultivation and magnetosome production has remained a challenge and requires the use of specific equipment and elaborate microoxic fermentation regimes. Thus, efforts were stimulated to genetically transfer the pathway for magnetosome biosynthesis to other non-magnetic hosts of biotechnological relevance that are easier to cultivate and can be grown to higher cell densities. So far, this approach has been successfully implemented only for two different non-magnetic *Alphaproteobacteria*: Compared to the relatively weak magnetization of hitherto non-magnetotactic strain *Magnetospirillum* sp. 15-1,[35] the phototrophic alphaproteobacterium *Rhodospirillum rubrum* has been efficiently endowed with the ability of magnetite biomineralization.[36] *R. rubrum* is relatively closely related to *M. gryphiswaldense*[37–39] with a 16S rRNA similarity of 90%,[36] and has gained increasing relevance in the field of biotechnology, for example, as production host for polyhydroxyalkanoates[40,41] or for hydrogen production.[42,43] The step-wise transfer of the five major magnetosome operons $mamAB_{op}$, $mamGFDC_{op}$, $mms6_{op}$, $mamXY_{op}$, and *feoAB1* of *M. gryphiswaldense* enabled the biosynthesis of magnetosome-like magnetite particles within the resulting transgenic strain *R. rubrum ABG6X_feoAB1* (in the following, referred to as *R. rubrum "magneticum"*).[36]

Magnetite biomineralization in *R. rubrum "magneticum"* occurred during microoxic chemotrophic as well as anoxic photoheterotrophic growth, for which the highest magnetic response was observed. Using the well-established Sistrom's minimal medium,[44,45] cultivation at moderate temperatures and light intensities resulted in the formation of up to 14 magnetosome particles per cell. However, the light-dependency of growth and magnetosome biosynthesis in *R. rubrum "magneticum"* were only preliminary investigated, and produced particles have not been fully characterized with respect to their physico-chemical properties. The feasibility to display foreign proteins on the surface of magnetosomes from *R. rubrum "magneticum"* by genetic engineering has been demonstrated by magnetosome expression of EGFP (enhanced green fluorescent protein) as fusion to MamC or MamJ, which resulted in fluorescent, filamentous particle chains within the cells.[36] However, it remained unexplored whether more complex, multimeric "cargo" proteins such as enzymes can be displayed as it has been shown for *M. gryphiswaldense*.[30,31]

In this study, we first explored different cultivation strategies with the aim to optimize magnetite biomineralization. We demonstrate that the combination of microoxic growth and a gradual increase of the light intensity adapted to increasing cell densities enable high-yield magnetosome production. Membrane-enveloped magnetosomes of up to 60 nm in diameter were synthesized, partially arranged in a chain-like manner within the cells. Moreover, as genetic engineering has proven to be a powerful approach for the functionalization of magnetosomes, we investigate whether established techniques can be assigned to *R. rubrum "magneticum"*. We show that functional moieties like the model enzyme glucuronidase GusA can be efficiently expressed on the magnetosomes surface, rendering the synthetic *R. rubrum "magneticum"* a promising host for high-yield production of functionalized magnetic nanoparticles with genetically engineerable properties.

2. Results and Discussion

2.1. Photoheterotrophic Growth Conditions Enable High-Yield Magnetosome Production in *R. rubrum "magneticum"*

Magnetosome formation in *R. rubrum "magneticum"* required microoxic chemotrophic or anoxic photoheterotrophic cultivation, but was most favored at medium light intensities (1000 lux) and temperatures (21–23 °C),[36] suggesting that magnetite biomineralization might rely on cellular processes and pathways induced and/or required for photosynthetic growth. Under these conditions, using Sistrom's minimal medium that employs succinate as sole carbon source and electron donor,[44,45] high levels of photosynthetic membranes were shown to be produced, which is in accordance with previous reports.[46,47] To further characterize and optimize magnetosome production, we tested different cultivation strategies and evaluated their effect on particle biosynthesis. First, we investigated the influence of the applied light intensity, which has been shown to crucially affect bacteriochlorophyll (BChl) synthesis in *R. rubrum*: Cells grown at low light intensities synthesized BChl and intracytoplasmic membrane (ICM) vesicles at higher rates compared to cells grown at high light intensity or chemotrophically in the dark,[46] and the formation of ICMs was inversely linked to the light intensity.[48] While in these studies the content of bacteriochlorophyll within ICMs remained nearly constant, *R. rubrum* adapted to a decrease in light intensity with an increase in

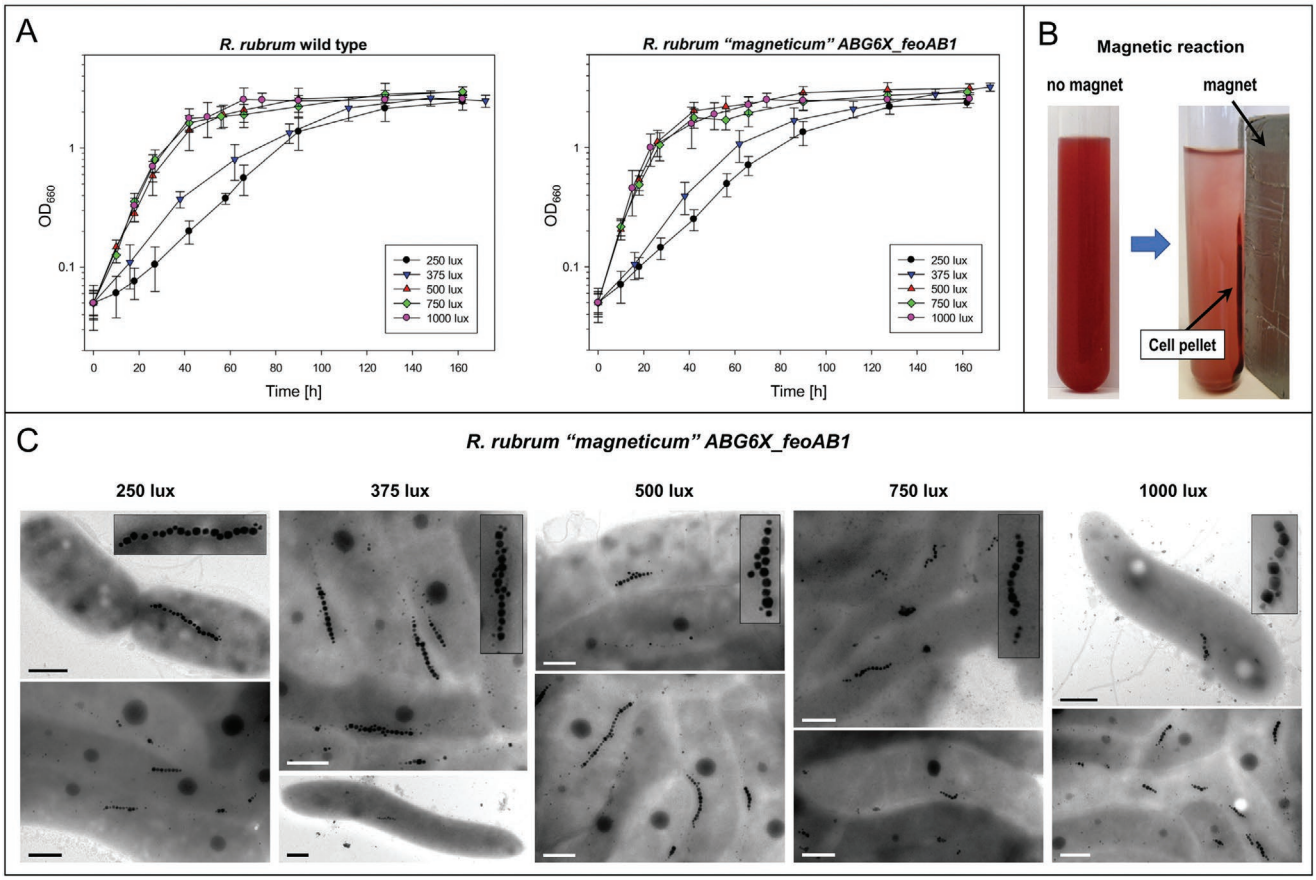

Figure 1. Magnetosome formation in *R. rubrum "magneticum"* under photoheterotrophic growth conditions applying different light intensities. Cultures were grown in Sistrom's minimal medium (supplemented with 50 μM Fe^{3+}) under microoxic conditions at 21 °C in 12 mL Hungate tubes. At the indicated light intensities (250–1000 lux) growth of the wild type of *R. rubrum* (A, left) and strain *"magneticum"* (A, right) were almost indistinguishable. While increased generation times were calculated for 250 and 375 lux, growth rates were nearly identical at light intensities above 500 lux. Standard deviations are based on at least three biological replicates ($n \geq 3$). B) Magnetic "response" of *R. rubrum "magneticum"* was indicated by accumulation of whole cells as a visible dark-red spot ("Cell pellet") near the pole of a permanent magnet at the edge of the Hungate tube. C) Transmission electron microscopy (TEM) images of representative cells indicate the formation of magnetosome chains (insets) to similar extents, thereby confirming the results of C_{mag} and iron measurements (Table 1). Scale bars = 0.5 μm.

ICM biosynthesis. As the underlying mechanisms and utilized determinants for magnetosome biosynthesis in *R. rubrum "magneticum"* are still unknown, the light intensity might also influence magnetite formation. We therefore performed growth experiments in Sistrom's minimal medium supplemented with 50 μM Fe^{3+} in 12 mL Hungate tubes under microoxic conditions and at 21 °C. Different light intensities ranging from 250 to 1000 lux were applied, and potential effects on growth, chromatophore synthesis, and magnetosome formation were evaluated. Cellular growth was monitored by measuring the optical density at 660 nm (OD_{660}; minimal BChl *a* absorption). OD_{880}/OD_{660} ratios served as metric for chromatophore synthesis as BChl *a* exhibits its absorption maximum at 880 nm.[48] The magnetic response (C_{mag}) of the cell suspensions served as indicator for magnetosome biosynthesis.[36,49] Thereby, the cells were aligned parallel to the field lines of a magnetic field, resulting in a change in light scattering ($\lambda = 660$ nm). The ratio of scattering intensities at different field angles relative to the light beam was used to characterize the average magnetic orientation of the cells. C_{mag} is well correlated with the average number of magnetosomes in magnetic cell populations and thus, can be used for semi-quantitative estimation of the magnetosome content.

For light intensities ranging from 250 to 1000 lux, *R. rubrum "magneticum"* exhibited growth rates and chromatophore biosynthesis comparable to those of the wild type (**Figure 1**A, **Table 1**). For both strains final optical densities (OD_{660}) of 2.4–3.2 and OD_{880}/OD_{660} ratios of 1.1–1.2 were measured. For dim-light intensities of 250 and 375 lux, generation times decreased to 16.2–16.8 h (250 lux) and 9.1–9.6 h (375 lux), whereas light intensities >500 lux led to generation times of ≈7.0–8.0 h. These values are similar as observed before for semi-aerobic cultures with succinate as sole carbon source.[50] Transmission electron microscopy (TEM) analyses revealed the presence of electron dense particles for all tested light intensities (i.e., 250, 375, 500, 750, or 1000 lux), with similar mean particle numbers per cell (as indicated by TEM micrographs, Figure 1C). However, magnetosomes were unevenly distributed within the respective populations: In some cells no or only few magnetosomes were observed, whereas others biomineralized

Table 1. Photoheterotrophic growth of the non-magnetic *R. rubrum* wild type (WT) and strain *"magneticum"* (Mag) at different light intensities. Cells were grown in 12 mL Hungate tubes under microoxic conditions at 21 °C applying the indicated light intensities. Once the stationary growth phase was reached (160 h), optical densities (OD_{660}), OD_{880}/OD_{660} ratios (indicator for bacteriochlorophyll biosynthesis) and generation times were determined. Magnetosome formation in strain *"magneticum"* is suggested by magnetic responses (C_{mag}) and the cellular Fe content (given as % of dry weight). Standard deviations are based on at least three biological replicates ($n \geq 3$).

Light intensity [lux]	250		375		500		750		1000	
	Mag	WT	Mag	WT	Mag	WT	Mag	WT	Mag	WT
OD_{660}	2.44 ± 0.36	2.38 ± 0.21	2.48 ± 0.29	3.22 ± 0.26	2.99 ± 0.26	3.15 ± 0.27	2.96 ± 0.30	2.92 ± 0.21	2.57 ± 0.21	2.56 ± 0.22
OD_{880}/OD_{660}	1.20	1.24	1.23	1.08	1.08	1.22	1.15	1.17	1.11	1.08
Generation time [h]	16.2 ± 2.1	16.8 ± 3.3	9.1 ± 0.7	9.6 ± 0.9	8.1 ± 0.4	7.6 ± 0.3	7.3 ± 0.4	7.0 ± 0.6	7.0 ± 0.3	6.6 ± 0.6
C_{mag}	0.44 ± 0.06	–	0.36 ± 0.08	–	0.47 ± 0.06	–	0.47 ± 0.08	–	0.43 ± 0.04	–
Fe content [% of dry weight]	0.17	0.04	0.15	0.04	0.18	0.04	0.19	0.20	0.14	0.01

chains of up to 25 particles per cell (Figure 1C). Furthermore, *R. rubrum "magneticum"* cells accumulated as a visible dark-red spot near the pole of a permanent magnet at the edge of the Hungate tube within few hours (Figure 1B). These observations are consistent with the increased cellular iron accumulation of magnetosome-producing cells (0.14–0.19% of cell dry weight) and C_{mag} values in the range from 0.36–0.47 (Table 1).

A further increase of the light intensity (1500–3500 lux) did not affect cellular growth (OD_{660} = 2.5 for 3500 lux), but inhibited magnetosome biosynthesis as indicated by reduced magnetic responses (Figure S1, Supporting Information). Since in the donor strain *M. gryphiswaldense* lower temperatures, which are suboptimal for growth, are known to favor magnetosome formation,[51] we investigated whether lower temperatures may counteract this effect or even enhance magnetosome biomineralization. Cultivation at 16 °C with light intensities of 1500–3500 lux resulted in optical densities OD_{660} in the range from 2.4–2.8 (which are similar to the values obtained for 21 °C; OD_{660} = 2.2–2.5) and generation times of ≈13 h on average (Figure S1, Supporting Information). Magnetic responses (C_{mag}) were nearly identical to the values obtained for 21 °C, ranging from 0.29 to 0.37. Aside from increased generation times (35–45 h), a further decrease of the cultivation temperature to 10 °C did not show any effects on the final optical density nor the C_{mag} values. Thus, reduced magnetosome biosynthesis at increased light intensities up to 3500 lux could not be compensated by lower growth temperatures, and remained behind those obtained for 21 °C and 1000 lux.

Next, we attempted to gradually increase the culture volume toward high-yield magnetosome production. For cultivation in 0.5 L flasks, again a light intensity of 1000 lux was applied. Cells were grown under microoxic conditions at 10 or 16 °C, and optical densities and magnetic responses were measured (Figure S2, Supporting Information). Under both conditions, final yields (OD_{660}) in the range from 1.9 to 2.5 were reached (**Table 2**). When grown at 16 °C, generation times of 18.1 ± 1.9 h were determined and OD_{880}/OD_{660} ratios were relatively constant (0.9–1.1). As expected, cultivation at 10 °C decelerated growth (generation time 65.4 ± 3.7 h), however, under these conditions the BChl content reached its maximum in the stationary phase (OD_{880}/OD_{660} = 1.2). In contrast to the cultivation in 12 mL Hungate tubes at 21 °C (for which similar C_{mag} values in the range from 0.4 to 0.5 were obtained), magnetic responses increased during cultivation, and for the applied light intensity of 1000 lux, C_{mag} values of up to 0.8 could be calculated, indicating enhanced magnetosome biosynthesis. These data suggest that at moderate illumination reduced cultivation temperatures (and thus reduced growth rates) favor magnetosome biosynthesis in *R. rubrum "magneticum"*. For further growth in upscaled culture volumes (2 or 10 L), we therefore applied a cultivation temperature of 10 °C. As illumination might become growth-limiting at larger volumes due to higher absorbance caused by increasing cell densities, we gradually increased the light intensity whenever growth rates or C_{mag} values declined (**Figure 2**). Thereby, a constant and sufficient illumination during the whole cultivation process could be ensured. Cultivation was started with light intensities of 300 lux (OD_{660} ≈0.03), which were further increased up to a final illumination rate of 1000 lux. For cultures of 2 L (Figure 2A, Table 2), a final optical density OD_{660} of 2.9 ± 0.1 and OD_{880}/OD_{660} ratios of ≈1.45 were obtained. Concomitantly, C_{mag} values could be increased to ≈1.4. For cultivation in 10 L flasks (**Figure 3**A) applying the same conditions, cells grew to an OD_{660} of 2.8 ± 0.6, and a magnetic response of ≈1.3 was reached (Figure 2B, Table 2).

Overall, our growth experiments demonstrated that low cultivation temperatures (10 °C) and light intensities ≤1000 lux favor magnetite biomineralization in *R. rubrum "magneticum"* as indicated by C_{mag} values. Under phototrophic conditions, BChl synthesis depends on light intensity and oxygen concentration. Thus, under microoxic/anoxic conditions and dim illumination, a high amount of ICM vesicles can be observed, accompanied by increased production rates for BChl and membrane proteins.[52] In addition, the cultivation temperature crucially affects photosynthetic reactions, as at low temperatures the electron transfer is restricted (although the charge separation is not critically affected).[53] Although the overall cellular protein content decreases proportionally with the temperature (for cultivation at ≤20 °C),[54] it can be assumed that under these conditions (as for the chromatophore synthesis) the folding and maturation of rather complex magnetosome proteins is favored.

Using this cultivation strategy under phototrophic conditions (i.e., at 10 °C and gradually increased light intensities), growth could be scaled-up to a final culture volume of 10 L (Figure 3A). TEM micrographs revealed the formation of 19 ± 7 particles per cell, with the majority being arranged in a chain-like manner (Figure 3 Bi and Bii; both showing representative

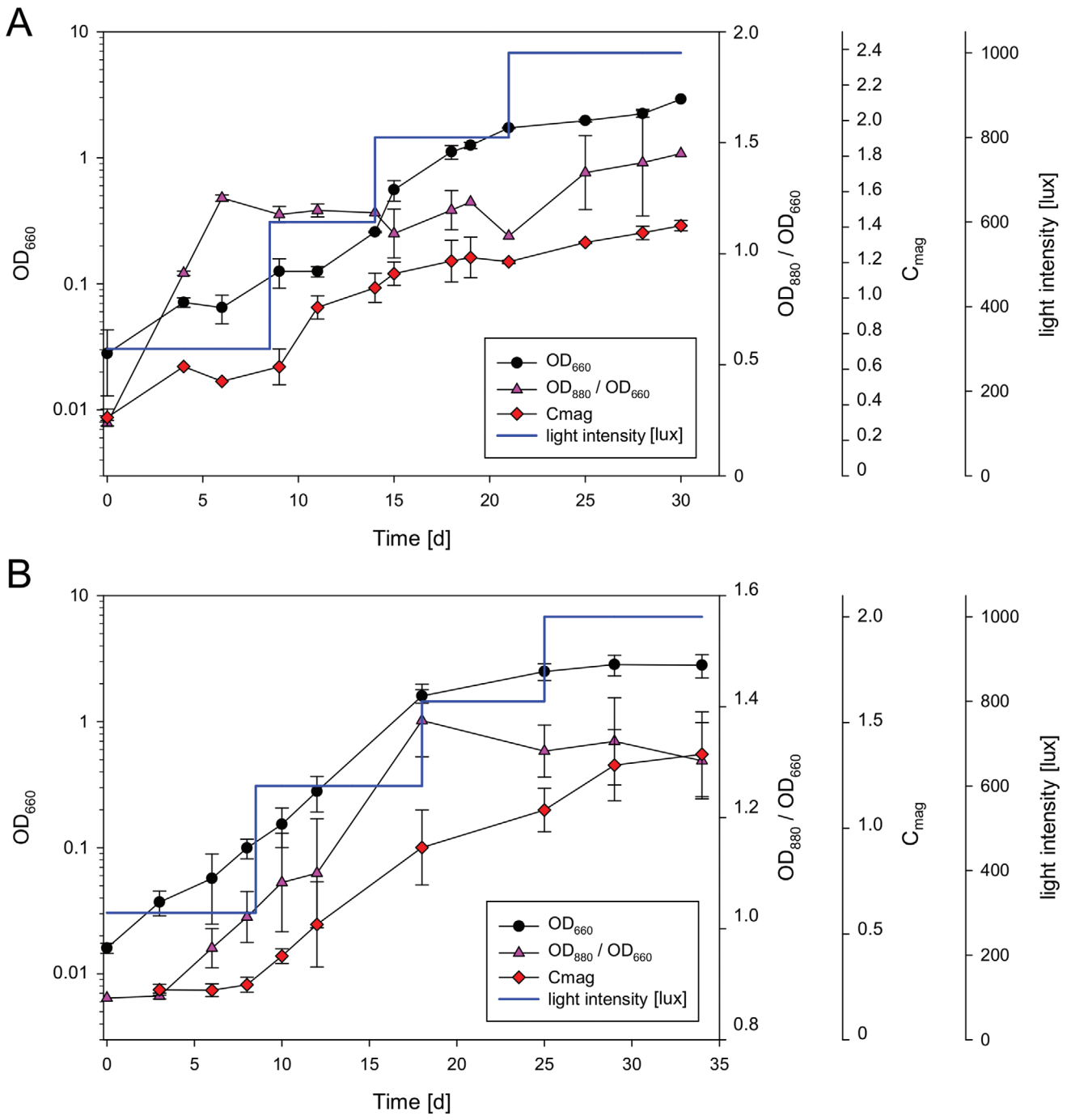

Figure 2. Photoheterotrophic cultivation of *R. rubrum "magneticum"* applying gradually increased light intensities. Cells were grown microoxically in A) 2 L or B) 10 L of Sistrom's minimal medium (supplemented with 50 µM Fe^{3+}) at 10 °C. In order to ensure a constant and sufficient illumination, light intensities were gradually increased whenever the growth rate declined or the magnetic response decreased. Standard deviations are based on at least three biological replicates ($n \geq 3$).

magnetosome producing cells). Thus, either one single or several shorter chains were observed, partially randomly distributed throughout the cell body. In dividing cells, particles were distributed to both daughter cells by splitting the magnetosome chain (Figure 3 Bii), similar to what has been observed for the donor strain *M. gryphiswaldense*.[2,55,56] However, the partially random positioning of the chains rather argues against a continuous MamK filament (although *mamK* is properly expressed in *R. rubrum "magneticum"*[36]) and in particular the formation of shorter chains might be explained by a combination of MamK-mediated chain assembly and magnetic attraction of single magnetosomes. This is also suggested by cryo-electron tomography (CET) (Figure 3 Ci), where no continuous MamK filament was visible or could be reconstructed

Table 2. Photoheterotrophic growth of *R. rubrum "magneticum"* in 0.5, 2, or 10 L of Sistrom's minimal medium. Cells were cultivated under microoxic conditions at the indicated cultivation temperatures. 0.5 L cultures were grown at 10 or 16 °C and 1000 lux. Since lower temperatures favored magnetosome biosynthesis (as indicated by C_{mag} values), cultures of 2 or 10 L were grown at 10 °C, and gradually increased light intensities (300–1000 lux) were applied to ensure constant and sufficient illumination during the cultivation process. The table summarizes the generation times, the final optical densities (OD_{660}), as well as OD_{880}/OD_{660} ratios and magnetic responses (C_{mag}) obtained in the stationary phase. Standard deviations are based on at least three biological replicates ($n \geq 3$).

Culture volume [L]	Cultivation temperature [°C]	Final OD_{660}	Final OD_{880}/OD_{660}	Generation time [h]	Final C_{mag}
0.5	16	2.56 ± 0.35	1.07 ± 0.11	18.1 ± 1.85	0.44 ± 0.19
	10	1.92 ± 0.39	1.22 ± 0.11	65.4 ± 3.68	0.75 ± 0.11
2	10	2.92 ± 0.10	1.45 ± 0.06	63.5 ± 5.24	1.41 ± 0.03
10	10	2.81 ± 0.59	1.30 ± 0.07	59.9 ± 3.66	1.35 ± 0.20

in the course of 3D rendering (Figure 3 Cii). Nevertheless, it cannot be discarded that MamK is present and is structured in a continuous manner, but was ablated away by the ion beam during the milling procedure to thin down the sample. In contrast, the cells contained densely packed vesicular ICMs (67.7 ± 14.9 nm in diameter), representing the photosynthetically active chromatophores.[57,58] In *R. rubrum*, the number of ICM vesicles within the cells is strongly influenced by the light intensity and oxygen concentration. At high light intensities the internal membranes are restricted to a peripheral location whereas at low light intensities the membranes are more abundant and intrude into the cytoplasm.[48,59,60] In a previous study, ICMs of ≈70 nm in diameter were formed under microoxic/anoxic conditions and low light intensities.[52] Thus, the high amount of ICMs observed by CET and their calculated diameters indicated high BChl synthesis rates.

For the isolation and purification of magnetosomes from *R. rubrum "magneticum"*, a method consisting of magnetic separation and a density-based ultracentrifugation step was applied, as previously described for the particle isolation from *M. gryphiswaldense*.[13,14] For *R. rubrum "magneticum"*, magnetosome isolation yielded an overall iron content of 9.82 ± 0.85 mg Fe per liter cell culture, which equals 0.55% of the cell dry weight. We subsequently performed small-angle X-ray scattering (SAXS) experiments to compare particle diameters and center-to-center distances of magnetosomes isolated from *R. rubrum "magneticum"* and the wild type of *M. gryphiswaldense* (Figure S4, Supporting Information). By analyzing the intensity profiles (and assuming a spherical particle shape), magnetosome mean core diameters with Gaussian distribution of 41 ± 7 nm (for *R. rubrum "magneticum"*) and 32 ± 5 nm (for *M. gryphiswaldense*) were obtained from the form factor minima. Based on the evaluation of a Bragg-like shoulder (highlighted by asterisks in Figure S4A, Supporting Information) observed at scattering vectors smaller than 0.015 $Å^{-1}$ average center-to-center distances *d* of 63 nm (*R. rubrum "magneticum"*) and 44 nm (*M. gryphiswaldense*) were determined. For further interpretation, a model based on polydisperse spheres with radius R for the iron oxide core (Figure S4B, Supporting Information) was applied to fit the profiles.[14,61] In this approach, the thickness of the biologic shell is approximated by half of the separation distance l (smallest distance from surface to surface of two spheres), i.e., by l/2. The fit yields R = 20.5 ± 3.5 nm and l = 22 nm for *R. rubrum "magneticum"*, and R = 16.0 ± 2.5 nm and l = 12 nm for *M. gryphiswaldense*. These values suggest that neighboring particles are in close contact with each other and are in a similar range as typical center-to-center distances previously observed for cell suspensions of *M. gryphiswaldense*. Furthermore, particle sizes are in accordance with values obtained by TEM analyses. For magnetosomes isolated from *R. rubrum "magneticum"*, an overall diameter of ≈45 nm (maximum 65 nm) was determined from electron micrographs, with the magnetite cores (40.3 ± 18.1 nm in diameter) being surrounded by an electron light organic shell of 6.0 ± 3.4 nm in thickness (**Table 3**), representing the magnetosome membrane (Figure 3D, inset, red arrows). Dynamic light scattering (DLS) measurements of highly diluted magnetosome suspensions resulted in increased particle diameters of 76.9 ± 28.3 nm (due to the presence of a hydrated shell that surrounds the particles). The zeta potential, which reflects the surface charge of isolated magnetosomes, was nearly identical to that of particles from *M. gryphiswaldense* (Table 3; *R. rubrum "magneticum"*: −33.6 ± 6.0 mV, *M. gryphiswaldense*: −33.9 ± 4.5 mV).

Besides single-crystalline particles with regular shapes that resembled magnetosomes from *M. gryphiswaldense*, a high number of particles with biomineralization defects was observed (Figure S5, Supporting Information). Specifically, only ≈62% of the particles from *R. rubrum "magneticum"* exhibited a single-crystalline domain structure and regular cuboctahedral shape, whereas more than one third of the crystals were twinned (19%), triplets (4%), or irregularly shaped (15%). Magnetite crystals with biomineralization defects can also be observed for magnetosomes from *M. gryphiswaldense*, but usually only to a minor degree.[2,3] Thus, our observations might indicate a partial misregulation of magnetosome biosynthesis in *R. rubrum "magneticum"* with regard to particle size and shape, which could be explained by an unbalanced magnetosome gene expression, effects or the lack of further determinants required for biomineralization, or combinations thereof. As observed for magnetosomes from *M. gryphiswaldense*, particle suspensions from *R. rubrum "magneticum"* could be attracted by external magnetic fields (ferrite or neodymium magnets) (Figure 3E), which points to a high saturation magnetization.

2.2. Genetic Functionalization of *R. rubrum* Magnetosomes by Expression of Fusion Proteins

Besides magnetosome expression of EGFP (as translational fusion to MamC or MamJ),[36] it remained unexplored whether

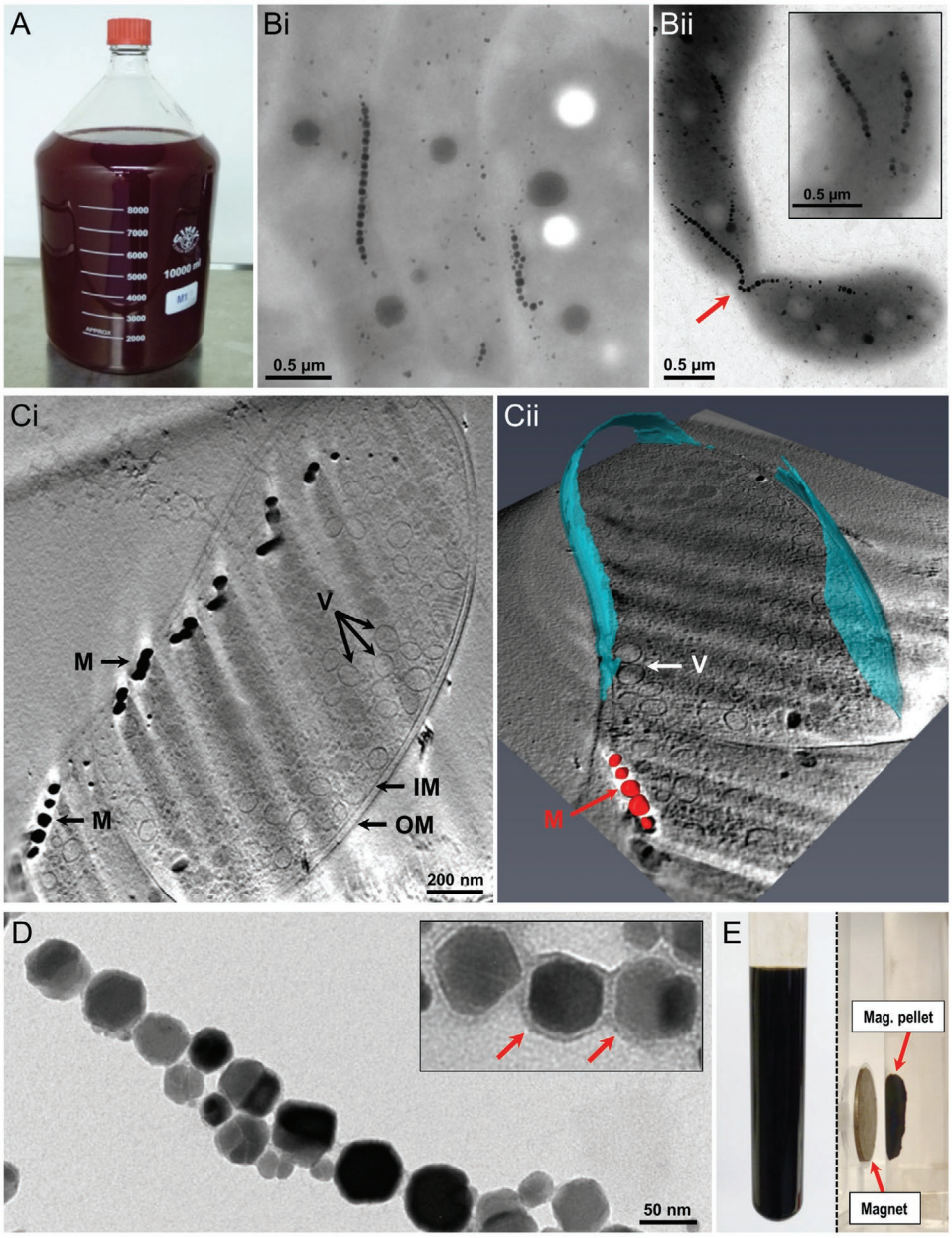

Figure 3. Magnetosome biosynthesis in *R. rubrum "magneticum"*. A) For high-yield magnetosome production, cells were grown under microoxic conditions in 10 L Sistrom's minimal medium, applying a cultivation temperature of 10 °C and gradually increased light intensities (300–1000 lux; depending on optical density and C_{mag}). Transmission electron microscopy analyses revealed the presence of up to 26 particles per cell, with the majority being arranged in one or several chains (Bi + Bii, both showing representative magnetosome producing cells). For dividing cells, TEM micrographs indicated particle partitioning to both daughter cells, partially by splitting the magnetosome chain (Bii, red arrow) as it has also been observed for *M. gryphiswaldense*.[56] TEM micrographs of the WT strain of *R. rubrum* (for comparison; grown under identical conditions) are provided in Figure S3, Supporting Information. Ci) Cryo-electron tomography image of a selected *R. rubrum "magneticum"* cell. A 15.7 nm thick tomographic slice (average of 5 slices of 3.132 nm thickness) revealing magnetosome formation and particle arrangement in a chain-like manner. M: magnetite crystal, IM: inner membrane, OM: outer membrane, V: vesicular, intracytoplasmic membranes (ICMs). Cii) CET 3D rendering of the cell shown in (Ci). Magnetite crystals (M) are shown in red, the cellular envelope inner and outer membranes are depicted in blue. Vesicular ICMs (V) are indicated by a white arrow. D) TEM micrograph of isolated magnetosomes. Particle suspensions were free of contamination and contained well-dispersed particles. In negatively stained preparations (inset), an electron-light organic shell was visible that surrounded the magnetosome cores (indicated by red arrows), representing the magnetosome membrane. E) Magnetosomes from *R. rubrum "magneticum"* can be attracted by magnetic fields. A suspension of isolated magnetosomes in a Hungate tube (left) was placed next to a permanent magnet (right), and the particles accumulated as a black spot ("Mag. pellet") near the pole of the magnet at the edge of the tube. Photoheterotrophic cultivation enabled high-yield particle production, with 9.82 ± 0.85 mg Fe per liter cell culture.

Table 3. Particle size and surface charge of magnetosomes isolated from *R. rubrum "magneticum"*. Cells were grown microoxically in 10 L Sistrom's minimal medium at 10 °C and gradually increased light intensities (300–1000 lux). After cell disruption, particles were isolated as previously described.[13,14] DLS analyses were applied to determine the overall magnetosome size. Measurements were performed on three biological replicates, and each replicate was measured in quintuplicates (n_{total} = 15). TEM micrographs were furthermore used to determine the overall magnetosome diameter, as well as the size of the magnetite core and the thickness of the surrounding magnetosome membrane ($n \geq 300$). In addition, the results obtained from volume-averaging SAXS measurements are provided, showing an excellent agreement between single particle and bulk analyses. Information on the surface charge of the particles is contained in the zeta potential. Particles were analyzed in 10 mM Hepes, pH 7.0. Values are compared to those obtained from magnetosomes isolated from *M. gryphiswaldense*.

Method	Magnetosomes origin		Comment
	M. gryphiswaldense	*R. rubrum "magneticum"*	
Overall diameter [nm]			
TEM	37.4 ± 6.2	44.7 ± 21.5	Dried, single particle characterization
DLS	61.5 ± 9.0	76.9 ± 28.3	Highly diluted, bulk characterization
SAXS	44.0 ± 7.5	63.0 ± 10.7	Concentrated suspension, bulk characterization
Detailed analysis			
Core diameter [nm]	34.8 ± 7.0	40.3 ± 18.1	TEM, dried
	32.0 ± 5.4	41.0 ± 7.0	SAXS, suspension
Membrane thickness [nm]	4.8 ± 1.7	6.0 ± 3.4	TEM, dried
	≤ 6 ± 1	≤ 11 ± 2	SAXS, suspension
Zeta potential [mV]	−33.9 ± 4.5	−33.6 ± 6.0	DLS, highly diluted

more complex "cargo" proteins can be genetically immobilized on the surface of magnetosomes from *R. rubrum "magneticum"*. To address this question, the well-characterized model enzyme glucuronidase GusA was chosen. The enzyme is easily assayed and catalyzes the hydrolysis of a variety of 3-glucuronides, yielding 3-glucuronates and an alcohol,[62,63] which can be monitored by absorption spectroscopy. For magnetosome display of GusA (**Figure 4**), Tn5-mediated transposition was used to insert a *mamC-gusA* gene fusion into the chromosome of *R. rubrum "magneticum"*. The pBam1-derived insertion plasmid harbors an expression cassette with the gene fusion under control of a transcriptional unit which has previously been used for constitutive high-level magnetosome expression of foreign proteins in the donor strain *M. gryphiswaldense*.[27,28]

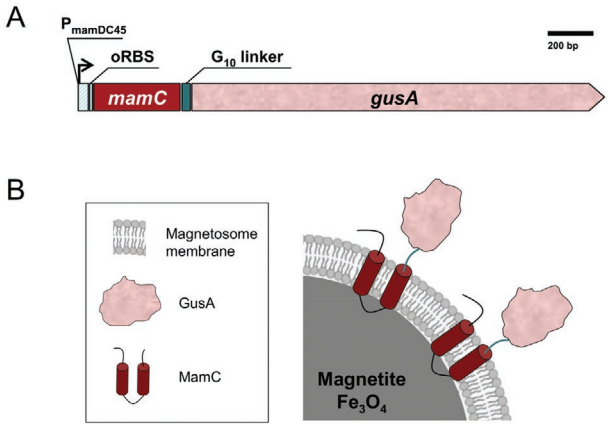

Figure 4. Magnetosome display of the model enzyme GusA in *R. rubrum "magneticum"*. A) Schematic representation showing the genetic organization of the *mamC-gusA* expression cassette for the magnetosome display of GusA. The *mamC-gusA* gene fusion was set under control of the $P_{mamDC45}$ promotor and a ribosome binding site (oRBS) both optimized for magnetosome expression of foreign moieties in the donor strain *M. gryphiswaldense*. B) The resulting particles displayed GusA monomers on the surface, which were genetically fused to MamC membrane anchors via flexible G_{10} linkers (size of particle and proteins not to scale).

Selected insertants of *R. rubrum_ABG6X_feoAB1_mamC-gusA* were undistinguishable from the parental strain *ABG6X_feoAB1* ("*magneticum*") with respect to cell morphology and magnetosome biosynthesis (**Figure 5**) and produced 21 ± 9 particles per cell, partially arranged in a chain-like manner. Expression of the MamC-GusA fusion protein was confirmed by subjecting the solubilized membrane proteins from the magnetosome fraction to denaturing polyacrylamide gel electrophoresis (PAGE), which was followed by Western blotting employing an immunoglobulin G (IgG) antibody against GusA (**Figure 6**A). During immunochemical detection, a distinct band of 87 kDa became visible, which corresponded well to the predicted molecular mass of the MamC-GusA fusion (81.6 kDa). A band of nearly identical mobility (albeit with less intensity) was obtained for MamC-GusA magnetosomes from *M. gryphiswaldense* (85 kDa), which were taken as control because they had been shown to display 47 copies of GusA on the surface (strain WT::*mamC-gusA*[30]). For commercial, soluble GusA a band with slightly increased mobility was detected (≈70 kDa), corresponding well to the calculated molecular mass of 68.3 kDa.

Remarkably, for the magnetosome fraction of *R. rubrum_ABG6X_feoAB1_mamC-gusA*, increased GusA protein amounts were detected compared to MamC-GusA magnetosomes isolated from a *M. gryphiswaldense* strain expressing the same construct (*R. rubrum_ABG6X_feoAB1_mamC-gusA*: 74 ng GusA/µg Fe, *M. gryphiswaldense* WT::*mamC-gusA*: 58 ng GusA/µg Fe[30]). This was rather unexpected as the increased diameters of the *R. rubrum* magnetosomes (≈45 nm) would drastically reduce the number of particles per µg magnetite. Assuming a roughly spherical particle shape and a density of magnetite of 5.24 g cm^{-3}, an average diameter of ≈45 nm would relate to a particle volume of 4.77×10^{-23} m^3 and a mass

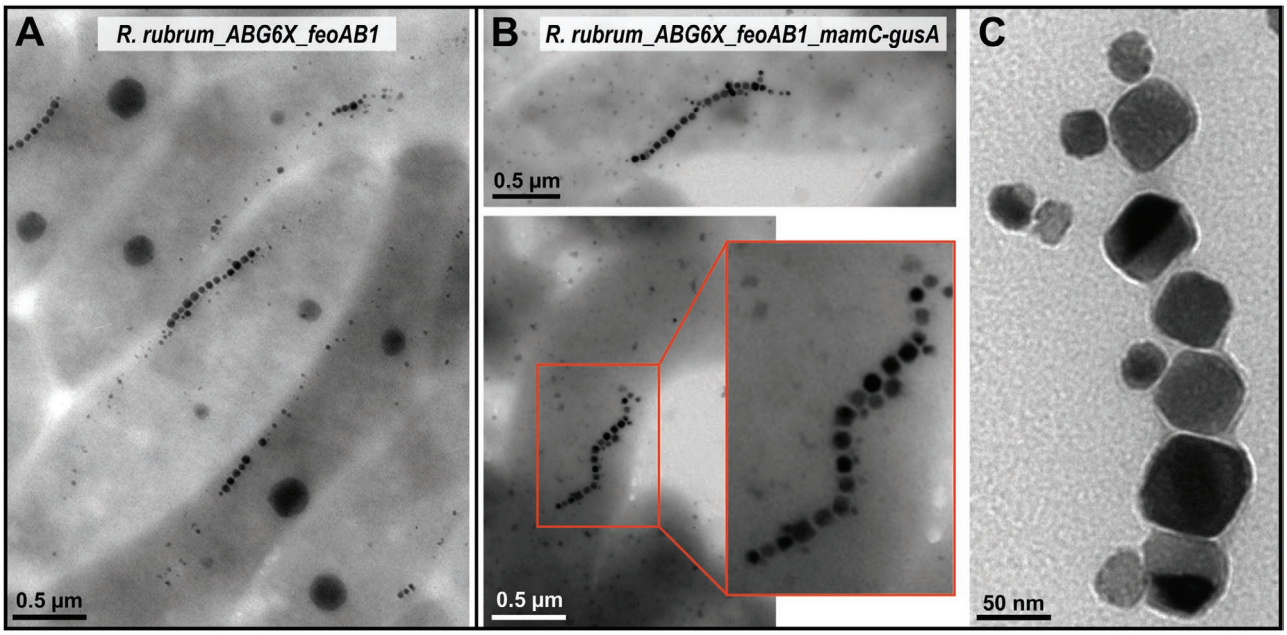

Figure 5. Transmission electron microscopy analyses of *R. rubrum_ABG6X_feoAB1_mamC-gusA* and the parental strain *R. rubrum_ABG6X_feoAB1* (*"magneticum"*). A) Under optimized photoheterotrophic growth conditions, the latter formed 19 ± 7 magnetosomes, partially arranged in a chain-like manner. B) Based on inspection by TEM, cells of strain *R. rubrum_ABG6X_feoAB1_mamC-gusA* were indistinguishable from *R. rubrum "magneticum"*, the chromosomal insertion of an additional *mamC-gusA* expression cassette did not influence biomineralization (21 ± 9 particles per cell). C) Suspensions of isolated magnetosomes from *R. rubrum_ABG6X_feoAB1_mamC-gusA* contained well-dispersed particles (up to 65 nm in diameter) with the magnetosome cores being surrounded by an electron light organic shell, hinting to an intact membrane.

of 2.50×10^{-16} g. Thus, $\approx 4.0 \times 10^9$ magnetosome particles per µg magnetite can be estimated, which is nearly only half of the value calculated for *M. gryphiswaldense* magnetosomes (diameter ≈36 nm, particle amount 7.8×10^9 per µg magnetite). Strikingly, based on the molecular mass of a single GusA monomer (68.3 kDa), a GusA protein amount of 119 molecules per magnetosome particle can be estimated. As strain *R. rubrum_ABG6X_feoAB1_mamC-gusA* harbors one unfused wild type copy of *mamC* and the additional *mamC-gusA* fusion (which are supposed to be equally abundant), this would result in ≈240 MamC membrane anchors per magnetosome. These data indicate that both the number of GusA monomers as well as the MamC copy number per particle were almost threefold increased compared to the values reported for *M. gryphiswaldense* WT::*mamC-gusA* (47 GusA monomers, ≈95 MamC copies[30]). Although the 1.4-fold increased surface of the *R. rubrum* magnetosomes would provide additional sites for the incorporation of magnetosome membrane anchors, the copy number of MamC seemed to be disproportionately increased for *R. rubrum* magnetosomes. Future studies will therefore focus on the architecture and the sub-proteome of the membrane of *R. rubrum* magnetosomes, and investigate if the relative abundances of the individual Mam proteins determined for *M. gryphiswaldense*[13] are retained.

Magnetosomes from *R. rubrum_ABG6X_feoAB1_mamC-gusA* exhibited glucuronide-hydrolyzing activity, which followed Michaelis–Menten kinetics (Figure 6B, Figure S6 and Table S1, Supporting Information). Thereby, reaction rates (v_{max}) and specific activities were increased compared to MamC-GusA magnetosomes from *M. gryphiswaldense* (**Table 4**), which is in accordance with the GusA protein amounts estimated from Western blots. Although the calculated K_M constants of 0.31 ± 0.01 mM were slightly increased compared to values reported for MamC-GusA magnetosomes from *M. gryphiswaldense* (0.17–0.19 mM[30]), the data still suggest a high affinity to the substrate *p*-nitrophenyl-*β*-D-glucuronide, indicating the presence of properly folded GusA on the magnetosome surface. As the enzyme is likely to be functional as a 272 kDa homotetramer,[64,65] the observed enzymatic activity furthermore suggests the successful oligomerization of monomeric GusA into functional oligomers. Thus, chromosomal insertion of a *mamC-gusA* cassette in *R. rubrum "magneticum"* resulted in GusA-decorated, catalytically highly active nanoparticles.

3. Conclusion

We systematically investigated photoheterotrophic growth of *R. rubrum "magneticum"* with the aim to optimize magnetosome biosynthesis. Conditions that favor BChl synthesis (i.e., low temperature and dim to moderate illumination) were found to enhance nanoparticle formation, suggesting that magnetite biomineralization might depend on redox activity, enzymes, or cofactors produced under photosynthetic conditions. Thereby, cellular processes that were identified as additional determinants for magnetite biomineralization in *M. gryphiswaldense* such as disulfide bond formation pathways for oxidative protein folding or cytochrome *c* biosynthesis[66] might be crucial. In *R. rubrum*, phototrophic growth relies on a cyclic electron transfer chain situated in chromatophores.[47,67,68] Thus, one

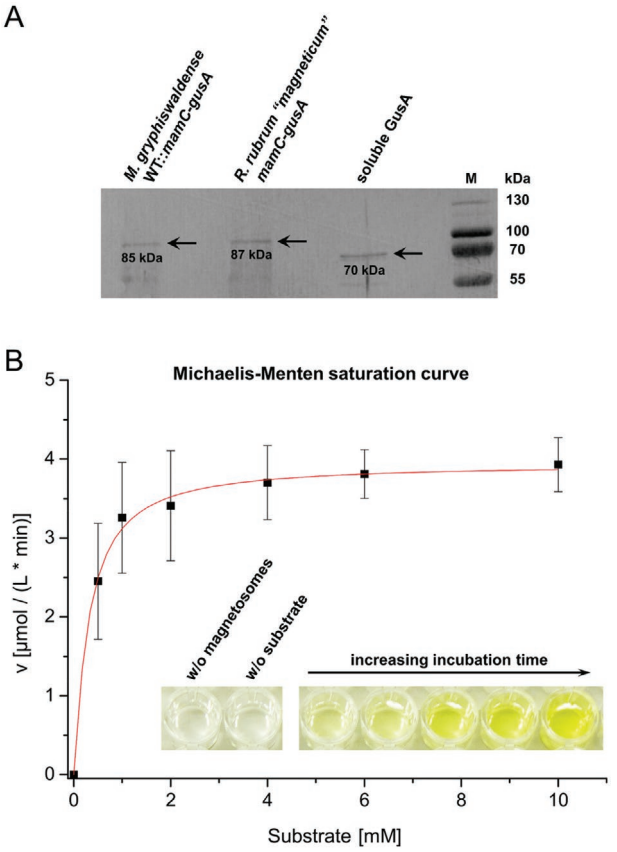

Figure 6. Magnetosome expression and catalytic activity of GusA immobilized on magnetosomes from *R. rubrum "magneticum"*. A) The solubilized protein fractions of isolated magnetosomes (10 µg of Fe species) from *R. rubrum_ABG6X_feoAB1_mamC-gusA* and *M. gryphiswaldense* WT::*mamC-gusA* (control[30]) were subjected to denaturing PAGE followed by quantitative Western blotting employing an IgG antibody directed against GusA. In both cases, bands of similar electrophoretic mobilities and thus, molecular masses (85–87 kDa) were obtained, which corresponded well to the predicted molecular mass of the MamC-GusA fusion protein (81.6 kDa). For commercial, soluble GusA (which was used as an additional control) a distinct band of ≈70 kDa was detected (calculated mass 68.3 kDa). M, protein molecular weight marker. B) GusA activity displayed by magnetosomes from *R. rubrum_ABG6X_feoAB1_mamC-gusA*. A modified protocol from Myronovskyi et al.[63] was used, which is based on the hydrolysis of the artificial substrate *p*-nitrophenyl-*β*-D-glucuronide. The time-dependent production of *p*-nitrophenol was monitored (inset), resulting in a characteristic yellow color. In the absence of magnetosomes ("w/o magnetosomes") or substrate ("w/o substrate") no absorption changes were observed. Absorption slopes were determined for different substrate concentrations and were subsequently taken to calculate reaction rates (v). The relation between substrate concentration and reaction rate for GusA magnetosomes isolated from *R. rubrum_ABG6X_feoAB1_mamC-gusA* is demonstrated by a Michaelis–Menten saturation curve. Error bars are based on at least three independent determinations ($n \geq 3$). Software Origin v7.0220 (OriginLab Corporation, Northampton, MA, USA) was used for curve fitting and determination of kinetic parameters K_M and v_{max} (see Table S1, Supporting Information).

can speculate that the latter supports a light-driven iron redox chemistry in *R. rubrum "magneticum"*, providing Fe^{2+}/Fe^{3+} species required for the formation of magnetite. In this respect, light-induced reactions between BChl and cytochromes (in particular their oxidation[69,70]) might be of particular importance. The transferred genes *mamP/E/T/X* from *M. gryphiswaldense* encode a series of predicted redox proteins that exhibit *c*-type cytochrome motifs (so-called magnetochrome (MCR) domains), and a participation of these MCR domains in an electron transfer chain has been suggested.[71] In *R. rubrum "magneticum"*, the biosynthesis of cytochrome cofactors during photosynthesis might favor MCR maturation, and photooxidative processes as well as accompanied electron transfer reactions might be linked to such MRC domains, thereby facilitating or even inducing the magnetite biomineralization process. Remarkably, enhancement of BChl synthesis rates alone did not increase cellular growth and particle yields. In preliminary experiments, chemotrophic growth at low oxygen levels (1% O_2) with succinate and fructose as carbon sources resulted in high levels of photosynthetic membranes (as it has been described in previous studies[47,50,72]), however, only poor magnetosome yields were obtained (data not shown). Similar observations were made before by Kolinko et al.,[36] again arguing for a light-driven magnetosome biosynthesis. Applying microoxic photoheterotrophic growth conditions that consider the mutual influence of the cultivation temperature and the employed light intensity, high-yield magnetosome production was achieved, rendering the synthetic *R. rubrum "magneticum"* a promising alternative to already established, culturable MTB. For *M. gryphiswaldense*, continuous improvements in bioreactor-based fermentation approaches have led to considerably increased cell densities and particle yields >35 mg magnetite per liter cell culture.[11,32–34,73] However, setting up fermentation regimes and combining the stable oxygen control with feeding strategies remains challenging. In our study, we investigated flask cultivation of *R. rubrum "magneticum"* under photoheterotrophic conditions, and the culture volume was scaled up to a final volume of 10 L. Reduced cultivation temperatures and a gradual increase of the applied light intensities led to high magnetosome yields of 9.82 mg Fe per liter cell culture, which equals 13.55 mg magnetite L^{-1}. Although these values were lower compared to *M. gryphiswaldense* cultivated in a bioreactor, particle yields were still more than fourfold increased compared to flask-cultivated *M. gryphiswaldense* (up to 3 mg per liter cell culture[74]).

In summary, our study investigated and characterized the synthetic *R. rubrum "magneticum"* as a suitable foreign host for recombinant magnetosome production. As magnetite biomineralization seemed to be linked to light-driven mechanisms induced for photoheterotrophic growth, *R. rubrum "magneticum"* could serve as a model organism for studying magnetosome biosynthesis under these conditions and for elucidating further auxiliary determinants. Furthermore, we show that magnetosomes from *R. rubrum "magneticum"* are fully accessible to genetic engineering, enabling the controlled decoration of the particle surface with functional moieties (as demonstrated by magnetosome expression of the model enzyme GusA). Since established engineering strategies for *M. gryphiswaldense* can easily be adopted and applied to *R. rubrum "magneticum"*, this approach provides the tools for engineering and production of bioconjugated magnetic nanoparticles with application potential in the biomedical and biotechnological field.

Table 4. GusA activity displayed by functionalized magnetosomes isolated from the engineered strains *R. rubrum_ABG6X_feoAB1_mamC-gusA* or *M. gryphiswaldense* WT::*mamC-gusA*. Particle amounts corresponding to 3.3 µg Fe species (Fe) were subjected to GusA activity assays, and kinetic parameters (K_M and ν_{max}) were calculated from Michaelis–Menten, Lineweaver–Burk, and Hanes–Woolf approximations. GusA protein amounts (estimated densitometrically from quantitative Western blots) were used to calculate specific enzymatic activities. Units (U) were defined as micromoles of product formed per minute and milligram of protein or Fe.

Strain	ng GusA/µg Fe	K_M [mM]	ν_{max} [µmol L^{-1} min^{-1}]	Specific activity	
				U mg^{-1} GusA	U mg^{-1} Fe
R. rubrum_ABG6X_feoAB1_mamC-gusA	74	0.31	4.00	16.54	1.22
M. gryphiswaldense WT::*mamC-gusA*[a)]	58	0.19	2.89	15.10	0.88

[a)]values taken from ref. [30].

4. Experimental Section

Bacterial Strains, Plasmids, and Cultivation Conditions: Bacterial strains and plasmids that were used in this study are listed in Tables S2 and S3, Supporting Information. Cultures of *R. rubrum* strains were cultivated in yeast extract-peptone-sulfur (YPS) medium (0.3% w/v yeast extract, 0.3% w/v peptone, 1 mM $CaCl_2$, and 1 mM $MgSO_4$) for heterotrophic growth,[75] or Sistrom's minimal medium for phototrophic growth,[44,45] supplemented with 50 µM Fe(III) citrate. *Escherichia coli* strains were grown as previously described.[76] For the cultivation of *E. coli* WM3064 D,L-α,ε-diaminopimelic acid was added to lysogeny broth medium at a final concentration of 1 mM. Strains were routinely cultured as previously described.[27] For the cultivation on solid medium, 1.5% (w/v) agar was added. For selection of antibiotic resistant strains, the following antibiotics concentrations were used: 25 µg mL^{-1} kanamycin (Kan) and 50 µg mL^{-1} ampicillin (Amp) for *E. coli* strains, and 25 µg mL^{-1} kanamycin and 300 µg mL^{-1} ampicillin for *R. rubrum* strains, respectively.

Molecular and Genetic Techniques: Oligonucleotides (see Table S4, Supporting Information) were purchased from Sigma Aldrich (Steinheim, Germany). For magnetosome expression of *gusA*, a pBAM1-derived vector harboring a *mamC-gusA* expression cassette under control of the optimized $P_{mamDC45}$ promotor and an optimized ribosome binding site[27] was transferred to *R. rubrum_ABG6X_feoAB1* via conjugation. The vector was constructed by cloning an additional ampicillin resistance cassette (*amp*) upstream of the *mamC-gusA* expression cassette into the AvrII/EcoRI restriction sites of pSB9, thereby generating pSB9_*amp*. Conjugation into *R. rubrum* was performed as described before[77] with the following modifications: Cultures were incubated heterotrophically in YPS medium at 30 °C under permanent illumination at 500 lux. ≈2×10^9 cells were mixed with 1×10^9 *E. coli* cells, spotted on YPS solid medium and incubated for 15 h. Cells were flushed from the plates and incubated on YPS agar medium supplemented with appropriate antibiotics for 7–10 days (Kan = 25 µg mL^{-1}, Amp = 300 µg mL^{-1}).

All constructs were sequenced by Macrogen Europe (Amsterdam, Netherlands). Sequence data were analyzed with Geneious 8.0.5 (Biomatters Ltd.) and ApE 2.0.47 (M. Wayne Davis, 2009).

Analytical Methods to Monitor Bacterial Growth and Magnetosome Biomineralization: The optical density (OD) of *R. rubrum* cultures was measured at 660 and 880 nm. The ratio OD_{880}/OD_{660} was used to estimate the chromatophore content within intact cells.[48] The average magnetic orientation of cell suspensions (C_{mag}) was assayed using an adapted light scattering assay (at λ = 660 nm) as described previously.[36,49] Briefly, for C_{mag} measurements, cells were aligned parallel to the field lines of a magnetic field, resulting in a change in light scattering. The ratio of the scattering intensities at different field angles relative to the light beam was used to characterize the average magnetic orientation of the cells and thus, as a proxy for the average number of magnetosomes in magnetic cell populations.

Contents of iron species from cells and isolated magnetosomes were determined by flame atomic absorption spectroscopy (AAS). Magnetosomes or cells (suspensions of equal optical densities) were pelleted, resuspended in 0.5 mL 69% (w/v) nitric acid and incubated at 98 °C for 3 h. The measurements were conducted with a Perkin–Elmer Atomic Absorption Spectrometer 1100 B (Überlingen, Germany) using the following conditions: wavelength 248.3 nm, gap width 0.2 nm, lamp current 20 mA.

Light intensities for phototrophic cultivation of *R. rubrum* strains were measured at the edge of the respective cultivation vessels using a LM-200 Lux meter (Eurolite, Germany) equipped with a silicon photodiode with filter (sampling rate two measurements per second).

Magnetosome Isolation and Purification: Isolation of magnetosomes from *R. rubrum "magneticum"* strains was performed as previously described.[13,14] Briefly, cells were harvested by centrifugation (10 500 × *g*, 4 °C, 30 min), and the cell pellets were resuspended in 50 mM Hepes, 1 mM ethylenediaminetetraacetic acid (EDTA), pH 7.2. For cell disruption, the suspension was passed three to five times through a microfluidizer system (M-110 L, Microfluidics Corp., Westwood, MA, USA) equipped with a H10Z interaction chamber at 124 MPa. Afterward, a magnetic separation step was performed, thereby loading the crude extract onto the magnetized matrix of a MACS column (5 mL; Miltenyi, Bergisch Gladbach, Germany). The magnetosomes were retained within the column, whereas non-magnetic cellular components were instantly diluted. For the further removal of impurities, the column was washed with 50 mL extraction buffer (10 mM Hepes, 1 mM EDTA, pH 7.2), followed by 50 mL high-salt buffer (10 mM Hepes, 1 mM EDTA, 150 mM NaCl, pH 7.2), and again 50 mL extraction buffer. Finally, the magnets were removed and the particles were eluted with ddH_2O. As an additional purification step, the magnetosome suspension was subjected to density-based ultracentrifugation (200 000 × *g*, 4 °C, 2 h) through a 60% (w/v) sucrose cushion. Due to their high density, the particles formed a pellet at the bottom of the tube, whereas residual impurities were retained in the cushion. Afterwards, the magnetosomes were resuspended in extraction buffer and stored in Hungate tubes at 4 °C under a nitrogen atmosphere.

TEM: For recording TEM images, suspensions of whole cells or isolated magnetosomes were adsorbed onto carbon-coated copper grids (Science Services, Munich, Germany). Magnetosome samples were additionally stained with 1% (w/v) uranyl acetate. TEM was performed on a CEM 902A (Zeiss, Oberkochen, Germany) with an acceleration voltage of 80 kV. Images were taken with a Gatan Erlangshen ES500W CCD camera. Crystal diameters were measured from TEM micrographs using the software ImageJ (version 1.48 v[78]).

Cryo-Electron Tomography (CET); Plunge-Freezing Vitrification: 4 µL of a *R. rubrum "magneticum"* culture (C_{mag}: 1.0, OD_{600} = 3.2, grown under anoxic and photosynthetic conditions) were mixed with 4 µL of 10 nm colloidal gold clusters (British Biocell International) used for subsequent alignment purposes. The mixture was added on glow-discharged Quantifoil R 2/1 holey carbon copper grids (Quantifoil Micro Tools GmbH, Jena, Germany), blotted, and embedded in vitreous ice by plunge-freezing into liquid ethane (< –170 °C) using a Vitrobot Mark 4 (FEI). The blotting conditions were set as blot force: 10, blot time: 3–5 s, drain time: 5 s, and humidity: 90%. The grids were stored in sealed boxes in liquid nitrogen until further use.

Cryo-Focused Ion Beam Sample Thinning: The plunge-frozen TEM grids were further processed in an FEI Quanta 3D FEG DualBeam FIB equipped

with a PP3000T cryo-system from Quorum Technologies.[79] Prior to FIB milling the sample was sputter-coated with Pt for 30 s at 10 mA in the FIB Quorum prep chamber to improve the sample conductivity. The wedge-milling geometry[80] was chosen as the preferred preparation technique for TEM grids containing only a low density of small cells. After rough milling using a Ga ion beam of 0.3 nA, and the subsequently performed thinning steps using stepwise reduced currents of 0.1 nA, 50 pA, and 30 pA, the final wedge angle was ≈5 degrees. Several such wedges were prepared on each of the grids. The grids were then again stored in sealed boxes in liquid nitrogen until used in the TEM.

CET: Tomography was performed as previously described[81] under low-dose conditions using a Tecnai F30 G^2 Polara transmission electron microscope (FEI) equipped with a 300 kV field emission gun, and a Gatan GIF 2002 post-column energy filter. For imaging, a 3838 × 3710 pixels Gatan K2 Summit Direct Detection Camera operated in dose-fractionation mode was used. Data were collected at 300 kV, with the energy filter operated in the zero-loss mode (slit width of 20 eV). Tilt series were acquired using Serial EM software.[82] The specimen was tilted about one axis with 1.5° increments over a typical total angular range of ±57°. The cumulative electron dose during the tilt series was kept below 150 e^- Å^{-2}. To account for the increased specimen thickness at high tilt angles, the exposure time was multiplied by a factor of 1/cos α. Pixel size at the specimen level was 5.22 Å at an EFTEM magnification of 22 500×. Images were recorded at nominal −5 µm defocus. Tomograms were reconstructed in the IMOD software package.[83] Tomographic reconstructions from tilt series were performed with the weighted back-projection with IMOD software using gold particles as a fiducial marker. An anisotropic non-linear diffusion denoising algorithm was used to improve signal-to-noise ratio. Segmentation was performed using Amira software on binned volumes with a voxel size of 31.32 Å. Membrane segmentation was done using the software TomoSegMemTV and a complementary package, SynapSegTools, both for Matlab.[84] Tomogram slices were obtained using 3dmod software from the IMOD package.

DLS Measurements: In addition to TEM, magnetosome sizes (hydrodynamic diameters) were determined by DLS using a Zetasizer Nano-ZS (Malvern, UK) at a wavelength of 638 nm in automatic mode at 25 °C. Measurements were performed on suspensions of isolated magnetosomes (from the wild type strain of *M. gryphiswaldense* or *R. rubrum "magneticum"*) in 10 mM Hepes, pH 7.0 and made in quintuplicates on three biological replicates (n_{total} = 15), using DTS1070 cuvettes (Malvern, UK). The evaluation software provided by the supplier (Malvern Zetasizer Software 7.13) is based on the Cumulant method and uses the Stokes–Einstein-Equation for size determination.

SAXS: For nanostructural SAXS-analyses, concentrated suspensions of isolated magnetosomes (in 10 mM Hepes/1 mM EDTA, pH 7.2) were filled into glass capillaries (∅ = 1 mm, Hilgenberg, Germany). The SAXS measurements were performed at ambient conditions using a Double Ganesha AIR system (SAXSLAB, Denmark). The monochromatic radiation with a wavelength of λ = 1.54 Å was produced by a rotating Cu anode (MicroMax 007HF, Rigaku Corporation, Japan). The position-sensitive detector (PILATUS 300 K, Dectris) was placed at different distances from the sample to cover a wide range of scattering vectors q, where q is given as $q = |\vec{q}| = \frac{4\pi}{\lambda}\sin\left(\frac{\theta}{2}\right)$ with λ representing the wavelength of the incident beam and θ the scattering angle. 1D intensity profiles of $I(q)$ versus q were obtained by radial averaging. All data were normalized to the intensity of the incident beam, the sample thickness, and the accumulation time. Background correction was performed by subtracting the signal of the diluent-filled capillary. The data were analyzed by applying the model of polydisperse spheres aligned in a chain-like manner,[61] using the software SasView 4.2.

Biochemical Methods: Polyacrylamide gels were prepared according to the method of Laemmli[85] and consisted of a 5% (w/v) acrylamide stacking gel and a 12% (w/v) running gel. Proteins of the solubilized magnetosome membrane fractions were separated by electrophoresis and subsequently transferred onto polyvinylidene difluoride membranes (Roth, Germany). Immunochemical detection was performed as described previously.[30,31] Briefly, for immunochemical detection of MamC-GusA fusion proteins, primary IgG antibodies specific for GusA (rabbit anti-GusA IgG primary antibodies; Antibodies-Online, Aachen, Germany) were applied at a 1:7500 ratio in alkaline phosphatase-tween (AP-T) buffer (0.1 M Tris; 0.1 M NaCl; 5 mM $MgCl_2 \times 6\ H_2O$; 0.05% (v/v) Tween 20; pH 7.4). After 2 h of incubation and removal of unbound/excess antibodies by several washing steps, the membrane was incubated with secondary goat anti-rabbit IgG antibodies with conjugated alkaline phosphatase (ratio 1:30 000 in AT-P buffer; Sigma Aldrich, Steinheim, Germany) for 1 h. For detection (after removal of unbound secondary antibodies), the membrane was transferred to a 5-bromo-4-chloro-3-indolyl-phosphate (BCIP)/nitro blue tetrazolium chloride substrate solution and incubated until violet bands appeared.

Spectrophotometric Measurement of Glucuronidase Activity: Enzymatic activity of GusA (β-glucuronidase from *E. coli*, EC 3.2.1.31) was determined by using a modified protocol from Myronovskyi et al.[63] GusA cleaves the artificial substrate *p*-nitrophenyl-β-D-glucuronide, yielding 3-glucuronate and *p*-nitrophenol. 1.0 mL (0.1–0.3 µg of iron (Fe) species as detected by AAS) of purified particles in dilution buffer (5 mM dithiothreitol (DTT), 0.1% Triton X-100, pH 7.0) were centrifuged and incubated at 37 °C for 15 min. The reaction was started by adding 5–100 µL 0.2 M *p*-nitrophenyl-β-D-glucuronide and carried out at 37 °C. The time-dependent production of *p*-nitrophenol was monitored, and the Michaelis–Menten constant K_M and maximal velocity v_{max} were calculated as the mean of Michaelis–Menten, Lineweaver–Burk, and Hanes–Woolf approximations (for details refer to, e.g., Johnson and Goody 2011[86]). Units (defined as U) were micromoles (µmol) of product formed per minute and milligram of protein or Fe. Reported values were averaged from at least three independent measurements ($n \geq 3$).

Statistical Analysis: Optical densities, iron contents, and magnetic responses were determined in biological/technical replicates as indicated. Data were reported as mean ± standard deviation. n represents the number of independent measurements. Statistical analyses were performed using SigmaPlot 12.0 software (Systat Software Inc., San Jose, CA, USA). For image processing, GIMP software (GNU Image Manipulation Program, version 2.8.16) was used. Magnetosome sizes were determined by DLS analysis (Zetasizer software 7.13, Malvern Instruments Ltd.). Measurements were performed on three biological replicates, and each replicate was analyzed in quintuplicates (n_{total} = 15). Particle sizes and membrane thicknesses were furthermore measured from TEM micrographs using the software ImageJ 1.48 v. The distance from the magnetite core to the surface of the organic layer was defined as membrane thickness. SAXS data were analyzed by applying the model of polydisperse spheres aligned in a chain-like manner,[61] using the software SasView 4.2. The protein amount of GusA in solubilized magnetosome membrane fractions was calculated densitometrically from quantitative Western blots using the software ImageJ. Origin v7.0220 software (OriginLab Corporation, Northampton, MA, USA) was used for drawing Michaelis–Menten saturation curves, curve fitting, and determination of kinetic parameters. GusA reaction rates (v_{max}) and Michaelis–Menten constants (K_M) were calculated as the mean of Michaelis–Menten, Lineweaver–Burk, and Hanes–Woolf approximations.

Supporting Information

Supporting Information is available from the Wiley Online Library or from the author.

Acknowledgements

The authors thank Sarah Borg for providing the *mamC-gusA* expression plasmid (pSB9) and Matthias Schlotter (Department of Microbiology, University of Bayreuth) for technical assistance with cell cultivation, magnetosome isolation, and iron measurements. Stephan Hauschild (Physical Chemistry 1, University of Bayreuth/Research Center Jülich GmbH, Jülich) is acknowledged for assistance with Zetasizer/DLS

measurements. The authors also thank Anne Augenstein, Victoria Clauß, Ingmar Pietsch, and Simon Markert for contributing DLS and SAXS data produced under the supervision of F.M. and S.R. during their academic studies at the Departments of Microbiology and Physical Chemistry I (University of Bayreuth).

A.S.S. acknowledges financial support from the Bavarian Academy of Sciences and Humanities (BAdW) via a Young Academy Fellowship. Further funding was received from the BMBF (MagBioFab to D.S.) and the European Research Council (ERC) under the European Union's Horizon 2020 research and innovation program (Grant No. 692637 to D.S.). This work benefited from the use of the SasView application, originally developed under NSF award DMR-0520547. SasView contains code developed with funding from the European Union's Horizon 2020 research and innovation program under the SINE2020 project, grant agreement No 654000.

Open access funding enabled and organized by Projekt DEAL.

Conflict of Interest

The authors declare no conflict of interest.

Data Availability Statement

Research data are not shared.

Keywords

genetic engineering, magnetic nanoparticles, magnetosomes, phototrophic cultivation, *Rhodospirillum rubrum*

Received: May 29, 2021
Revised: July 10, 2021
Published online: July 23, 2021

[1] C. Jogler, D. Schüler, *Annu. Rev. Microbiol.* **2009**, *63*, 501.
[2] R. Uebe, D. Schüler, *Nat. Rev. Microbiol.* **2016**, *14*, 621.
[3] A. Lohße, S. Borg, O. Raschdorf, I. Kolinko, É. Tompa, M. Pósfai, D. Faivre, J. Baumgartner, D. Schüler, *J. Bacteriol.* **2014**, *196*, 2658.
[4] R. Hergt, R. Hiergeist, M. Zeisberger, D. Schüler, U. Heyen, I. Hilger, W. A. Kaiser, *J. Magn. Magn. Mater.* **2005**, *293*, 80.
[5] M. Bennet, L. Bertinetti, R. K. Neely, A. Schertel, A. Körnig, C. Flors, F. D. Müller, D. Schüler, S. Klumpp, D. Faivre, *Faraday Discuss.* **2015**, *181*, 71.
[6] R. Taukulis, M. Widdrat, M. Kumari, D. Heinke, M. Rumpler, É. Tompa, R. Uebe, A. Kraupner, A. Cebers, D. Schüler, M. Pósfai, A. Hirt, D. Faivre, *Magnetohydrodynamics* **2015**, *51*, 721.
[7] U. Heyen, D. Schüler, *Appl. Microbiol. Biotechnol.* **2003**, *61*, 536.
[8] Y. Li, E. Katzmann, S. Borg, D. Schüler, *J. Bacteriol.* **2012**, *194*, 4847.
[9] Y. Li, M. Sabaty, S. Borg, K. T. Silva, D. Pignol, D. Schüler, *BMC Microbiol.* **2014**, *14*, 153.
[10] Y. Li, O. Raschdorf, K. T. Silva, D. Schüler, *J. Bacteriol.* **2014**, *196*, 2552.
[11] C. N. Riese, R. Uebe, S. Rosenfeldt, A. S. Schenk, V. Jérôme, R. Freitag, D. Schüler, *Microb. Cell Fact.* **2020**, *19*, 206.
[12] M. Boucher, F. Geffroy, S. Prévéral, L. Bellanger, E. Selingue, G. Adryanczyk-Perrier, M. Péan, C. T. Lefèvre, D. Pignol, N. Ginet, S. Mériaux, *Biomaterials* **2017**, *121*, 167.
[13] O. Raschdorf, F. Bonn, N. Zeytuni, R. Zarivach, D. Becher, D. Schüler, *J. Proteomics* **2018**, *172*, 89.
[14] S. Rosenfeldt, F. Mickoleit, C. Jörke, J. H. Clement, S. Markert, V. Jérôme, S. Schwarzinger, R. Freitag, D. Schüler, R. Uebe, A. S. Schenk, *Acta Biomater.* **2021**, *120*, 293.
[15] R. Weissleder, A. Moore, U. Mahmood, R. Bhorade, H. Benveniste, E. A. Chiocca, J. P. Basilion, *Nat. Med.* **2000**, *6*, 351.
[16] W. S. Seo, J. H. Lee, X. Sun, Y. Suzuki, D. Mann, Z. Liu, M. Terashima, P. C. Yang, M. V. McConnell, D. G. Nishimura, H. Dai, *Nat. Mater.* **2006**, *5*, 971.
[17] D. Heinke, A. Kraupner, D. Eberbeck, D. Schmidt, P. Radon, R. Uebe, D. Schüler, A. Briel, *Int. J. Magn. Part. Imaging* **2017**, *3*, 1706004.
[18] A. Kraupner, D. Eberbeck, D. Heinke, R. Uebe, D. Schüler, A. Briel, *Nanoscale* **2017**, *9*, 5788.
[19] R. Hergt, R. Hiergeist, M. Zeisberger, D. Schüler, U. Heyen, I. Hilger, W. A. Kaiser, *J. Magn. Magn. Mater.* **2005**, *293*, 80.
[20] E. Alphandéry, S. Faure, O. Seksek, F. Guyot, I. Chebbi, *ACS Nano* **2011**, *5*, 6279.
[21] E. Alphandéry, F. Guyot, I. Chebbi, *Int. J. Pharm.* **2012**, *434*, 444.
[22] C. Sun, J. S. H. Lee, M. Zhang, *Adv. Drug Delivery Rev.* **2008**, *60*, 1252.
[23] E. Alphandéry, D. Abi Haidar, O. Seksek, F. Guyot, I. Chebbi, *Nanoscale* **2018**, *10*, 10918.
[24] T. Tanaka, T. Matsunaga, *Anal. Chem.* **2000**, *72*, 3518.
[25] T. Tanaka, H. Takeda, F. Ueki, K. Obata, H. Tajima, H. Takeyama, Y. Goda, S. Fujimoto, T. Matsunaga, *J. Biotechnol.* **2004**, *108*, 153.
[26] N. Ginet, R. Pardoux, G. Adryanczyk, D. Garcia, C. Brutesco, D. Pignol, *PLoS One* **2011**, *6*, e21442.
[27] S. Borg, J. Hofmann, A. Pollithy, C. Lang, D. Schüler, *Appl. Environ. Microbiol.* **2014**, *80*, 2609.
[28] F. Mickoleit, D. Schüler, *Bioinspired, Biomimetic Nanobiomater.* **2019**, *8*, 86.
[29] J. Xu, L. Liu, J. He, S. Ma, S. Li, Z. Wang, T. Xu, W. Jiang, Y. Wen, Y. Li, J. Tian, F. Li, *J. Nanobiotechnol.* **2019**, *17*, 37.
[30] F. Mickoleit, D. Schüler, *Adv. Biosyst.* **2018**, *2*, 1700109.
[31] F. Mickoleit, C. Lanzloth, D. Schüler, *Small* **2020**, *16*, 1906922.
[32] Y. Zhang, X. Zhang, W. Jiang, Y. Li, J. Li, *Appl. Environ. Microbiol.* **2011**, *77*, 5851.
[33] A. Fernández-Castané, H. Li, O. R. T. Thomas, T. W. Overton, *New Biotechnol.* **2018**, *46*, 22.
[34] C. Berny, R. Le Fèvre, F. Guyot, K. Blondeau, C. Guizonne, E. Rousseau, N. Bayan, E. Alphandéry, *Front. Bioeng. Biotechnol.* **2020**, *8*, 16.
[35] M. V. Dziuba, T. Zwiener, R. Uebe, D. Schüler, *Environ. Microbiol.* **2020**, *22*, 1603.
[36] I. Kolinko, A. Lohße, S. Borg, O. Raschdorf, C. Jogler, Q. Tu, M. Pósfai, É. Tompa, J. M. Plitzko, A. Brachmann, G. Wanner, R. Müller, Y. Zhang, D. Schüler, *Nat. Nanotechnol.* **2014**, *9*, 193.
[37] M. Richter, M. Kube, D. A. Bazylinski, T. Lombardot, F. O. Glöckner, R. Reinhardt, D. Schüler, *J. Bacteriol.* **2007**, *189*, 4899.
[38] C. Jogler, G. Wanner, S. Kolinko, M. Niebler, R. Amann, N. Petersen, M. Kube, R. Reinhardt, D. Schüler, *Proc. Natl. Acad. Sci. USA* **2011**, *108*, 1134.
[39] C. T. Lefèvre, D. Trubitsyn, F. Abreu, S. Kolinko, L. G. P. de Almeida, A. T. R. de Vasconcelos, U. Lins, D. Schüler, N. Ginet, D. Pignol, D. A. Bazylinski, *Environ. Microbiol.* **2013**, *15*, 2267.
[40] H. Jin, B. J. Nikolau, *PLoS One* **2014**, *9*, e96621.
[41] G. Bayon-Vicente, S. Zarbo, A. Deutschbauer, R. Wattiez, B. Leroy, *Appl. Environ. Microbiol.* **2020**, *86*, e00901.
[42] S. S. Hosseini, M. Aghbashlo, M. Tabatabaei, H. Younesi, G. Najafpour, *Energy* **2015**, *93*, 730.
[43] M. F. Tiang, M. A. F. Hanipa, P. M. Abdul, J. M. Jahim, S. S. Mahmod, M. S. Takriff, C.-H. Lay, A. Reungsang, S.-Y. Wu, *Int. J. Hydrogen Energy* **2020**, *45*, 13211.
[44] W. R. Sistrom, *Microbiology* **1960**, *22*, 778.
[45] W. R. Sistrom, *J. Gen. Microbiol.* **1962**, *28*, 607.

[46] G. Cohen-Bazire, R. Kunisawa, *J. Cell Biol.* **1963**, *16*, 401.
[47] H. Grammel, E. D. Gilles, R. Ghosh, *Appl. Environ. Microbiol.* **2003**, *69*, 6577.
[48] S. C. Holt, A. G. Marr, *J. Bacteriol.* **1965**, *89*, 1421.
[49] D. Schüler, U. Rainer, E. Bäuerlein, *FEMS Microbiol. Lett.* **1995**, *132*, 139.
[50] R. Ghosh, A. Hardmeyer, I. Thoenen, R. Bachofen, *Appl. Environ. Microbiol.* **1994**, *60*, 1698.
[51] E. Katzmann, M. Eibauer, W. Lin, Y. Pan, J. M. Plitzko, D. Schüler, *Appl. Environ. Microbiol.* **2013**, *79*, 7755.
[52] G. Schön, R. Jank-Ladwig, *Arch. Microbiol.* **1972**, *85*, 319.
[53] T. Odahara, N. Ishii, A. Ooishi, S. Honda, H. Uedaira, M. Hara, J. Miyake, *Biochim. Biophys. Acta* **2011**, *1808*, 1645.
[54] I. Kaiser, J. Oelze, *Arch. Microbiol.* **1980**, *126*, 187.
[55] E. Katzmann, A. Scheffel, M. Gruska, J. M. Plitzko, D. Schüler, *Mol. Microbiol.* **2010**, *77*, 208.
[56] M. Toro-Nahuelpan, F. D. Müller, S. Klumpp, J. M. Plitzko, M. Bramkamp, D. Schüler, *BMC Biol.* **2016**, *14*, 88.
[57] M. L. Collins, R. A. Niederman, *J. Bacteriol.* **1976**, *126*, 1326.
[58] J. M. Noble, J. Lubieniecki, B. H. Savitzky, J. M. Plitzko, H. Engelhardt, W. Baumeister, L. F. Kourkoutis, *Mol. Microbiol.* **2018**, *109*, 812.
[59] G. Schön, R. Ladwig, *Arch. Mikrobiol.* **1970**, *74*, 356.
[60] R. L. Uffen, R. S. Wolfe, *J. Bacteriol.* **1970**, *104*, 462.
[61] S. Rosenfeldt, C. N. Riese, F. Mickoleit, D. Schüler, A. S. Schenk, *Appl. Environ. Microbiol.* **2019**, *85*, e01513.
[62] R. A. Jefferson, S. M. Burgess, D. Hirsh, *Proc. Natl. Acad. Sci. USA* **1986**, *83*, 8447.
[63] M. Myronovskyi, E. Welle, V. Fedorenko, A. Luzhetskyy, *Appl. Environ. Microbiol.* **2011**, *77*, 5370.
[64] A. B. Roberts, B. D. Wallace, M. K. Venkatesh, S. Mani, M. R. Redinbo, *Mol. Pharmacol.* **2013**, *84*, 208.
[65] B. D. Wallace, A. B. Roberts, R. M. Pollet, J. D. Ingle, K. A. Biernat, S. J. Pellock, M. K. Venkatesh, L. Guthrie, S. K. O'Neal, S. J. Robinson, M. Dollinger, E. Figueroa, S. R. McShane, R. D. Cohen, J. Jin, S. V. Frye, W. C. Zamboni, C. Pepe-Ranney, S. Mani, L. Kelly, M. R. Redinbo, *Chem. Biol.* **2015**, *22*, 1238.
[66] K. T. Silva, M. Schüler, F. Mickoleit, T. Zwiener, F. D. Müller, R. P. Awal, A. Weig, A. Brachmann, R. Uebe, D. Schüler, *mSystems* **2020**, *5*, e00565.
[67] B. LaSarre, D. T. Kysela, B. D. Stein, A. Ducret, Y. V. Brun, J. B. McKinlay, *mBio* **2018**, *9*, e00780.
[68] J. N. Sturgis, R. A. Niederman, in *The Purple Phototrophic Bacteria*, Springer, Dordrecht **2009**, pp. 253.
[69] W. S. Zaugg, *Proc. Natl. Acad. Sci. USA* **1963**, *50*, 100.
[70] E. S. Lindstrom, *Plant Physiol.* **1962**, *37*, 127.
[71] M. I. Siponen, G. Adryanczyk, N. Ginet, P. Arnoux, D. Pignol, *Biochem. Soc. Trans.* **2012**, *40*, 1319.
[72] L. Carius, O. Hädicke, H. Grammel, *Biotechnol. Bioeng.* **2013**, *110*, 573.
[73] J. B. Sun, F. Zhao, T. Tang, W. Jiang, J. S. Tian, Y. Li, J. L. Li, *Appl. Microbiol. Biotechnol.* **2008**, *79*, 389.
[74] D. Schüler, E. Baeuerlein, *J. Phys. IV* **1997**, *7*, 647.
[75] P. F. Weaver, J. D. Wall, H. Gest, *Arch. Microbiol.* **1975**, *105*, 207.
[76] J. Sambrook, D. Russell, *Molecular Cloning: A Laboratory Manual*, 3rd ed., Cold Spring Harbor Laboratory Press, New York **2001**, pp. 1–44.
[77] I. Kolinko, C. Jogler, E. Katzmann, D. Schüler, *J. Bacteriol.* **2011**, *193*, 5328.
[78] T. J. Collins, *BioTechniques* **2007**, *43*, S25.
[79] M. Schaffer, B. D. Engel, T. Laugks, J. Mahamid, J. M. Plitzko, W. Baumeister, *Bio-Protoc.* **2015**, *5*, e1575.
[80] E. Villa, M. Schaffer, J. M. Plitzko, W. Baumeister, *Curr. Opin. Struct. Biol.* **2013**, *23*, 771.
[81] D. Pfeiffer, M. Toro-Nahuelpan, M. Bramkamp, J. M. Plitzko, D. Schüler, *mBio* **2019**, *10*, e02716.
[82] D. N. Mastronarde, *J. Struct. Biol.* **2005**, *152*, 36.
[83] J. R. Kremer, D. N. Mastronarde, J. R. McIntosh, *J. Struct. Biol.* **1996**, *116*, 71.
[84] A. Martinez-Sanchez, I. Garcia, S. Asano, V. Lucic, J.-J. Fernandez, *J. Struct. Biol.* **2014**, *186*, 49.
[85] U. K. Laemmli, *Nature* **1970**, *227*, 680.
[86] K. A. Johnson, R. S. Goody, *Biochemistry* **2011**, *50*, 8264.